A Bio-Realistic Analog CMOS Cochlea Filter With High Tunability and Ultra-Steep Roll-Off

Shiwei Wang, *Student Member, IEEE*, Thomas Jacob Koickal, Alister Hamilton, Rebecca Cheung, *Senior Member, IEEE*, and Leslie S. Smith, *Senior Member, IEEE*

***Abstract*—This paper presents the design and experimental results of a cochlea filter in analog very large scale integration (VLSI) which highly resembles physiologically measured response of the mammalian cochlea. The filter consists of three specialized sub-filter stages which respectively provide passive response in low frequencies, actively tunable response in mid-band frequencies and ultra-steep roll-off at transition frequencies from pass-band to stop-band. The sub-filters are implemented in balanced ladder topology using floating active inductors. Measured results from the fabricated chip show that wide range of mid-band tuning including gain tuning of over 20dB, Q factor tuning from 2 to 19 as well as the bio-realistic center frequency shift are achieved by adjusting only one circuit parameter. Besides, the filter has an ultra-steep roll-off reaching over 300 dB/dec. By changing biasing currents, the filter can be configured to operate with center frequencies from 31 Hz to 8 kHz. The filter is 9^{th} order, consumes $59.5 \sim 90.0\ \mu$W power and occupies $0.9\ \mathrm{mm}^2$ chip area. A parallel bank of the proposed filter can be used as the front-end in hearing prosthesis devices, speech processors as well as other bio-inspired auditory systems owing to its bio-realistic behavior, low power consumption and small size.**

***Index Terms*—Analog VLSI, auditory filter, bio-inspired circuits, CMOS cochlea, floating active inductor.**

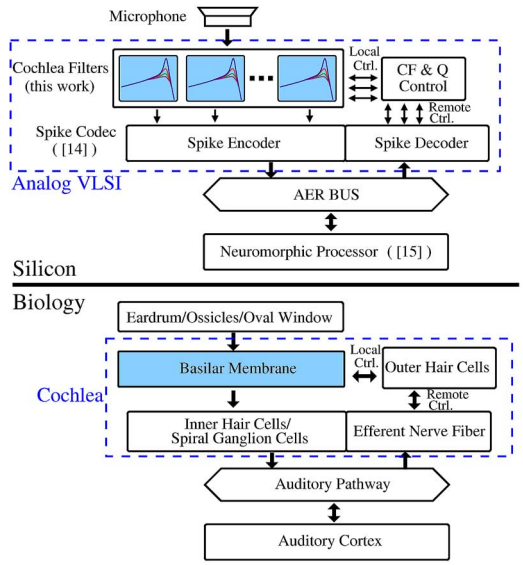

Fig. 1. Position of this work in a bio-inspired auditory system, in comparison with system-level diagram of biological auditory system.

I. Introduction

THE cochlea in the inner ear of mammals has remarkable filter functions. It converts sound pressure into multi-channels of band-passed outputs, where the sensitivity of each channel is dynamically tuned according to the input intensity and the out-of-band frequency components are greatly suppressed with an ultra-steep roll-off at the stop-band [1]. These filtering features of cochlea make it capable of adapting to wide dynamic range of sound input and performing high-resolution frequency decomposition. In recent years, many bio-inspired systems employing filters that emulate the cochlea filter functions have been implemented, which are used in a variety of applications including hearing prosthetic devices [2]–[4], speech/sound recognition systems [5]–[10] as well as RF spectrum analyzers [11] and channel multiplexers [12]. In this work, we aim to build a cochlea filter in analog VLSI which closely resembles the frequency response of biological cochlea. The use of analog circuitry for front-end signal processing improves power-efficiency [13] (see position of the cochlea filters in Fig. 1). Besides, the progressive results from physiological experiments on the biological cochlea [16]–[25], [27], [28] have provided us with deeper understanding of the cochlea behavior which brings more inspiration to build filters that behave faithfully to biology.

In fact, analog VLSI models of the cochlea have been studied for over two decades and a number of systems have been implemented [29]–[42]. These systems generally consist of filter banks based on second-order sections (SOS) in different configurations including cascade [29]–[35], parallel [36]–[38] and 2-dimensional (2-D) topology [39]–[42]. The filter cascade structure models the wave propagation in the basilar membrane of cochlea using from 32 to 120 stages of SOS connected in series [29], [30], [32]–[34]. Gain and filter roll-off steepness are accumulated with the long cascade, which provides good similarity with biological frequency response. Nevertheless, the cascade structure suffers from the accumulation of both noise and delays, and also, failure of one stage in the cascade will affect all of its following stages. On the contrary, the parallel

Manuscript received January 29, 2014; revised April 23, 2014; accepted May 29, 2014. This work was supported by EPSRC, U.K., under Grants to the University of Edinburgh (EP/G063710/1), and to the Universityof Stirling (EP/G062609/1). The China Scholarship Council provided support for the first author. This paper was recommended by Associate Editor S.-C. Liu.

S. Wang, T. J. Koickal, A. Hamilton, and R. Cheung are with the Institute for Integrated Micro and Nano Systems, University of Edinburgh, EH9 3JL Edinburgh, U.K. (e-mail: shiwei.wang@ed.ac.uk).

L. S. Smith is with the Department of Computer Science and Mathematics, University of Stirling, FK9 4LA Stirling, U.K.

Color versions of one or more of the figures in this paper are available online at http://ieeexplore.ieee.org.

Digital Object Identifier 10.1109/TBCAS.2014.2328321

structure avoids these drawbacks by employing independent filter channels, and the number of SOS stages in each channel is limited to 1 or 2 [36]–[38]. However, as the filter complexity is significantly reduced in each channel, its frequency response is no longer comparable with that observed in the biological cochlea. The 2-D topology solves the problems in both noise and delay accumulation and bio-fidelity. It agrees with the parallel structure in the aspect that SOS stages are configured in a parallel manner, and only one SOS stage is used for each channel [39]–[42]. However, the channels are not independent of each other but are coupled through a resistive network which models the effects of cochlea fluid, and the coupling between the channels results in fairly faithful response compared with biology [40]–[42]. Nevertheless, while the usability of the 2-D topology designs has not been convincingly proven, the cascade and parallel structures have already been used in a variety of audio processing tasks [43]–[45] and particularly, the feasibility of the parallel structure in cochlea implant products has been sufficiently demonstrated [36], [37], [46].

In this work, we aim to improve the performance of the parallel structure in terms of bio-faithful frequency tuning and roll-off steepness. A filter channel which closely emulates the frequency response measured from biological cochlea is developed to replace the simple band-pass filters used in the existing parallel designs [36]–[38]. The filter is designed by directly following the implications from recent physiological experiments. Inspired by the fact that the biological cochlea has separate response features from low to high frequencies [1], the proposed design consists of three cascaded sub-filter stages, which respectively resemble the passive response in low frequencies, active response in mid-band frequencies and steep roll-off in transition frequencies. The use of specialized sub-filters increases overall efficiency, reducing filter tuning complexity and filter order required to achieve bio-faithful response. The sub-filters are built in balanced ladder topology using floating active inductors, which reduces the design complexity. The proposed cochlea filter is superior to the gammatone-based design [47] in terms of ease of analog VLSI implementation and bio-realism of frequency response. Besides, the filter can directly interface with microphone output, unlike the design reported in [48] which has to be operated with a floating current source as input.

The paper is organized as following. The system-level filter structure is introduced in Section II. The details of circuit implementation are discussed in Section III. The circuit non-idealities are analyzed in Section IV. The measured chip results are discussed in Section V, followed by a conclusion of the paper in Section VI.

II. System Design

Physiological experiments [1], [16]–[18], [21] indicate that magnitude frequency response of the basilar membrane in biological cochlea has an asymmetric shape and highly active behavior. It has a gentle slope in the low-frequency band (in the region of 20 dB/dec [1], [17], [18]) and a highly steep roll-off at the stop-band (330 dB/dec or even higher [1], [16]–[18]). In the mid-band, the gain, selectivity and center frequency increases with decreasing input strength: the increase of gain can

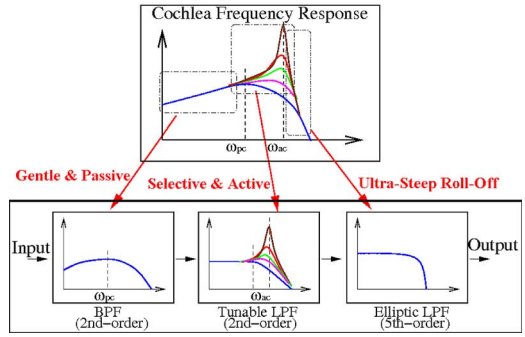

Fig. 2. System architecture. Each of the three sub-filters emulates one stage of the biological cochlea frequency behavior.

reach in the range of $20 \sim 40$ dB [16]–[18], [21], the maximum Q factor can reach as high as 10 [16]–[18], [21], and the center frequency increases by over 40% [1], [16]–[18], [21]. Generally speaking, the response is gentle and passive in low frequencies, selective and active in mid-band frequencies and steep in the transition from pass-band to stop-band, which indicates the frequency response of cochlea can be divided into three stages from low to high frequencies as first suggested in [1]. Based on this observation, a filter architecture composed of three cascaded sub-filters, each of which represents one stage of the cochlea response, is proposed as shown in Fig. 2. A biquad band-pass filter (BPF) whose center frequency determines the passive center frequency of the entire cochlea filter presents the gentle and passive response, a biquad low-pass filter (LPF) with tunable gain, Q factor and center frequency presents the active and selective response, and an elliptic filter which has sharpest transition among all filter types presents the steep roll-off. To match the steepness of roll-off slope, the elliptic filter is designed as 5^{th}-order and the entire cochlea filter is a 9^{th}-order system.

III. Circuit Implementation

A. Basic Cell: Floating Active Inductor (FAI)

Among the three filters proposed to build a cochlea filter, it is the high order elliptic filter that brings most design difficulty and challenge. For audio frequencies, implementation of passive LC-ladder topology in VLSI is unrealistic due to unfeasibly large size of passive inductors. Active RC [49] and switch-capacitor implementations [50] require the same number of op-amps with the filter order, and are thus constrained by power consumption. Reported log-domain implementations mostly use bipolar transistors targeting at high frequency applications [51], [52], while the CMOS implementations are either low-order [53], [54] or not proven with chip results [55]–[57].

Therefore, we developed a floating active inductor (FAI) as the basic cell to build active LC ladders, which is shown in Fig. 3. The FAI is inspired by several existing active inductor designs in [58], and has been modified so that it operates in floating mode as required by LC ladders. Also, the circuits are designed to operate in weak inversion so as to achieve the long time constant for audio frequencies. The FAI is based on gyrator-C topology. The transistor pair MN and MP respectively

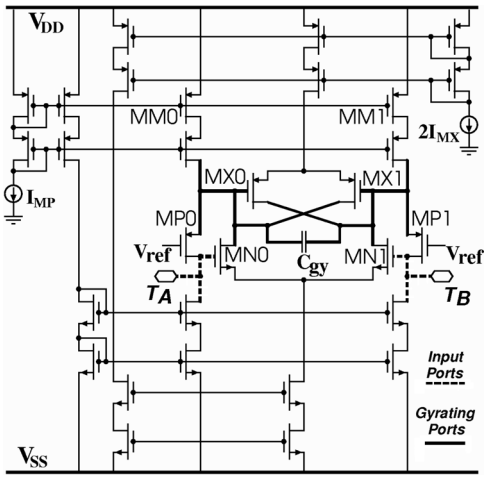

Fig. 3. Schematic of FAI. The basic cell for implementation of ladder filters. Three differential transistor pairs MP, MN and MX and a load capacitor C_{gy} are configured in gyrator-C topology. The input ports and gyrating ports of the FAI are highlighted.

provide the forward and reverse transconductance to form a gyrator, and C_{gy} is the capacitor loaded at the gyrating ports. The transistor pair MX functions as a compensation transconductor which reduces the resistive loading that the sources of the MP transistors add on the gyrating ports. The quality factor of the FAI is tunable by adjusting the transconductance difference between the MP pair and MX pair. More details about the FAI cell have been provided in [59]. The FAI-based active LC ladders are not only used to build the steep roll-off 5^{th} order elliptic filter, but also the BPF and LPF sub-filters shown in Fig. 2.

Deriving from [59], the equivalent impedance of the FAI is given by

$$Z(s) = \frac{4C_{gy} \cdot s}{g_{MP}g_{MN}} + \frac{2(g_{MP} - g_{MX})}{g_{MP}g_{MN}} \tag{1}$$

where g_{MP}, g_{MN} and g_{MX} are the transconductance of the transistor pairs. Substrates of MN, MP and MX pairs are all connected to power supplies, and as sources of MX0-MX1 and MN0-MN1 pairs are respectively tied together, the body effect does not have much influence on their differential transconductance. However, MP0 and MP1 have separate sources and thus the body effect transconductance g_{mb} should be considered. The transistors operate in weak inversion and thus g_{mb} approximately equals $n - 1/n \cdot I_D/U_T$ [60] where n is slope factor, I_D is biasing drain current and U_T is thermal voltage. Besides, the currents in MN and MX are made equal as shown in Fig. 3. Thus, the equivalent inductance and resistance can be written as

$$L = \frac{4C_{gy}nU_T^2}{I_{MP}I_{MX}} \tag{2}$$

$$R = \frac{2U_T(nI_{MP} - I_{MX})}{I_{MP}I_{MX}}. \tag{3}$$

Equations (2) and (3) show that the FAI inductance and resistance can be tuned by adjusting I_{MP} and I_{MX}.

The drain-source conductance (g_{ds}) due to channel length modulation is not considered. Because in weak inversion $g_{ds} = I_D/\lambda L$ will be at least one hundred times smaller than the transistor transconductance $g_m = I_D/nU_T$ according to the process parameters (λ is channel length modulation parameter and L is transistor channel length).

B. Triple-Stage Cochlea Filter Design Based on FAI

Based on the FAI cell, 2^{nd} order BPF, 2^{nd} order LPF, 5^{th} order elliptic filters and their cascaded cochlea filter channel are built as shown in Fig. 4. The BPF is built by loading a fully differential OTA (FDOTA: Fig. 5) with two FAIs and a capacitor, and the LPF is built upon FAI-C voltage divider with a fully differential difference amplifier (FDDA: Fig. 6) as input buffer, while the elliptic filter is built according to filter design handbook [61] with single-end OTAs (OTA: Fig. 7) providing equivalent source resistance. There are a total of eight FAIs in each channel, and their I_{MP} currents are made equal through current mirrors, while I_{MX} currents are set separately. We denote the I_{MP} currents as I_{STAT}, and I_{MX} as I_{BPF}, I_{LPF} and I_{ELLI} respectively. The FDOTA and the single-end OTA also operate in weak inversion and are biased with $2I_{STAT}$ currents. The FAIs in BPF and LPF are all loaded with equal capacitance of C_0, while C_{BPF} is set as 1.2 C_0 and C_{LPF} is set as C_0.

Thereby the transfer functions of BPF and LPF are derived as

$$H_{BPF}(s) = \frac{5I_{STAT}}{6nU_TC_0} \cdot \frac{s + \omega_{z,BPF}}{s^2 + \frac{\omega_{0,BPF}}{Q_{BPF}}s + \omega_{0,BPF}^2} \tag{4}$$

$$\begin{cases} \omega_{z,BPF} = \frac{nI_{STAT} - I_{BPF}}{2nU_TC_0} \\ \omega_{0,BPF} = \frac{1}{4nU_TC_0}\sqrt{\frac{5}{3}nI_{STAT}I_{BPF}} \\ Q_{BPF} = \frac{1}{2(nI_{STAT} - I_{BPF})}\sqrt{\frac{5}{3}nI_{STAT}I_{BPF}} \end{cases} \tag{5}$$

$$H_{LPF}(s) = \omega_{0,LPF}^2 \cdot \frac{1}{s^2 + \frac{\omega_{0,LPF}}{Q_{LPF}}s + \omega_{0,LPF}^2} \tag{6}$$

$$\begin{cases} \omega_{0,LPF} = \frac{1}{4nU_TC_0}\sqrt{2nI_{STAT}I_{LPF}} \\ Q_{LPF} = \frac{1}{2(nI_{STAT} - I_{LPF})}\sqrt{2nI_{STAT}I_{LPF}} \end{cases}. \tag{7}$$

The transfer function of the elliptic filter can be derived by obtaining poles and zeros from filter design tables [61]. In our design, the elliptic filter is 5^{th} order, with the reflection coefficient $\rho = 5\%$, the modular angle $\theta = 36^\circ$ and power loss factor $K^2 = \infty$, which in theory can achieve pass-band ripple of 0.01 dB, steepness factor of 1.7013 and minimum stop-band attenuation of 40.81 dB (equivalent to cut-off slope of 176.8 dB/dec). The transfer function of the elliptic filter is given in (8) at the bottom of the next page, where $\omega_{-3\,\mathrm{dB}}$ is the -3 dB corner frequency.

We can also obtain the parameters of filter elements by referring to the filter design tables in [61]. By setting $\omega_{-3\,\mathrm{dB}}$ as $\sqrt{2}$

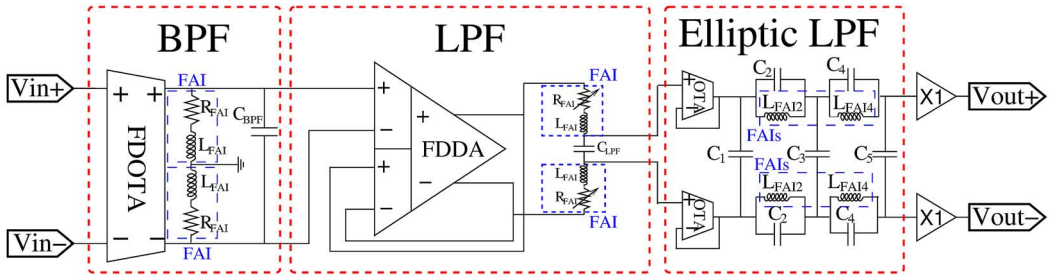

Fig. 4. Detailed structure of the cochlear filter channel consisting of three sub-filters. FAIs and capacitors are used to create the balanced ladder topologies.

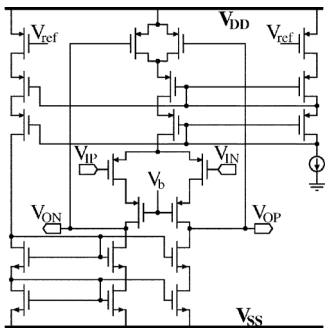

Fig. 5. Schematic of the fully differential operational transconductance amplifier (FDOTA).

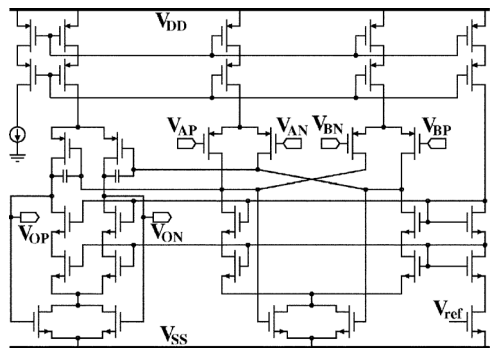

Fig. 6. Schematic of the fully differential difference amplifier (FDDA).

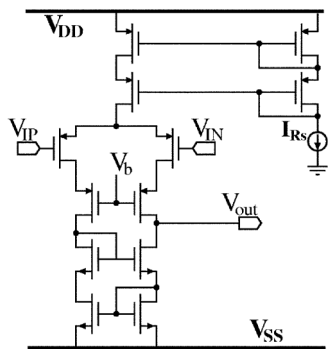

Fig. 7. Schematic of the single-end OTA. Its DC current I_{Rs} sets the source resistance of the elliptic filter.

times of $\omega_{0,BPF}$ (center frequency of BPF), the values of required inductance and capacitance can be derived as following:

$$\begin{cases} L_{FAI2} = 0.8551(\frac{nU_T}{I_{STAT}})^2\sqrt{\frac{I_{STAT}}{nI_{BPF}}}C_0 \\ L_{FAI4} = 1.113(\frac{nU_T}{I_{STAT}})^2\sqrt{\frac{I_{STAT}}{nI_{BPF}}}C_0 \end{cases} \tag{9}$$

$$\begin{cases} C_1 = 0.5252\sqrt{\frac{I_{STAT}}{nI_{BPF}}}C_0 \\ C_2 = 0.7651\sqrt{\frac{I_{STAT}}{nI_{BPF}}}C_0 \\ C_3 = 2.296\sqrt{\frac{I_{STAT}}{nI_{BPF}}}C_0 \\ C_4 = 1.373\sqrt{\frac{I_{STAT}}{nI_{BPF}}}C_0 \\ C_5 = 2.293\sqrt{\frac{I_{STAT}}{nI_{BPF}}}C_0 \end{cases}. \tag{10}$$

Combining (2) and (9), the values of C_{gy} in FAI2 and FAI4 can be derived

$$\begin{cases} C_{gy,FAI2} = 0.2138(\frac{I_{ELLI}}{I_{STAT}})\sqrt{\frac{nI_{STAT}}{I_{BPF}}}C_0 \\ C_{gy,FAI4} = 0.2783(\frac{I_{ELLI}}{I_{STAT}})\sqrt{\frac{nI_{STAT}}{I_{BPF}}}C_0 \end{cases}. \tag{11}$$

In the cochlea filter channel, only I_{LPF} is actively tuned, while I_{BPF} and I_{ELLI} kept constant. Based on exhaustive simulations with extracted parameters in software, we choose to make I_{BPF} equals I_{STAT} so that the BPF has a relatively low Q factor and gentle response, and I_{ELLI} equals $1.2I_{STAT}$ so that the FAIs in the elliptic filter are inductive enough to maintain the steep roll-off while enough margin is left to avoid negative-damping and instability. In addition, we use $x = I_{LPF}/I_{STAT}$ to denote the tuning factor of the LPF and also the entire cochlea filter, which can be dynamically controlled to mimic the active response of the biological cochlea. The transfer functions can be greatly simplified if we use ω_{pc} (the passive center frequency of the cochlea filter)

$$H_{ELLI}(s) = \frac{0.069851\omega_{-3\,\mathrm{dB}} \cdot (s^2 + 7.3381\omega_{-3\,\mathrm{dB}}^2)(s^2 + 3.1407\omega_{-3\,\mathrm{dB}}^2)}{(s + 0.96232\omega_{-3\,\mathrm{dB}})(s^2 + 1.2360\omega_{-3\,\mathrm{dB}}s + 1.1724\omega_{-3\,\mathrm{dB}}^2)(s^2 + 0.34350\omega_{-3\,\mathrm{dB}}s + 1.4269\omega_{-3d\,\mathrm{dB}}^2)} \tag{8}$$

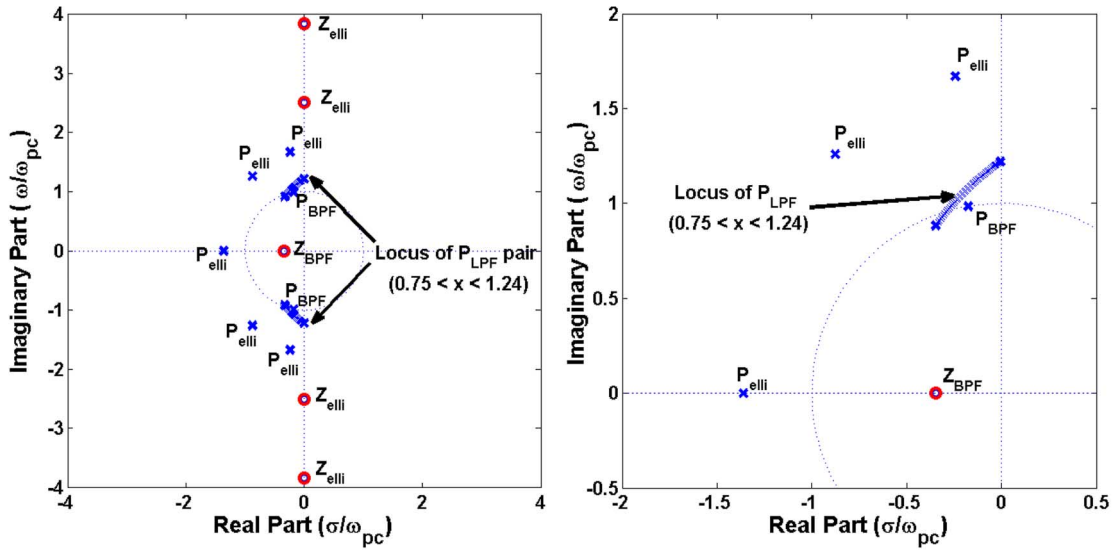

(a) (b)

Fig. 8. (a) Normalized pole-zero plot of the proposed cochlea filter channel. (b) Pole-zero plot zoomed to left-up corner.

to replace $\omega_{0,BPF} = 1/4nU_TC_0\sqrt{5/3nI_{STAT}I_{BPF}}$. Combining (4), (6) and (8) with the above mentioned design settings ($\omega_{-3\,\mathrm{dB}} = \sqrt{2}\,\omega_{0,BPF}$, $I_{BPF} = I_{STAT}$, $x = I_{LPF}/I_{STAT}$, $I_{ELLI} = 1.2\ I_{STAT}$), the transfer function of the cascaded cochlea filter channel can be derived as (12) at the bottom of the page. As the slope factor n in AMS 0.35 μm process is approximately 1.25, (12) can be further simplified into (13) at the bottom of the page. The proposed filter has nine poles and five zeros and its normalized zero-pole plot is shown in Fig. 8. As there are no zeros in the right half of the s-plane, the cochlea filter is a minimum-phase filter, as is the biological cochlea [63].

IV. Analysis of Non-Idealities

A. Mismatch

Naturally, the operation of the FAI is subject to transistor mismatches which cause circuit offsets. The mismatches can be classified into two categories: horizontal and vertical. The horizontal mismatch is the mismatch between transistors in differential pairs MP0-MP1, MN0-MN1 and MX0-MX1 which results in a DC current in the FAI running from port TA to TB. Taking the differential pair MN as an example, shown in Fig. 9(a), the mismatch between MN0 and MN1 will cause deviation in their transconductance, which results in a DC current running from

$$
\begin{aligned}
H_{tot}(s) = {} & (2.31\omega_{pc} \cdot \frac{s + 1.55\frac{n-1}{\sqrt{n}}\omega_{pc}}{s^2 + 1.55\frac{n-1}{\sqrt{n}}\omega_{pc}s + \omega_{pc}^2}) \\
& \cdot (\frac{1.2x\omega_{pc}^2}{s^2 + 1.55\frac{n-x}{\sqrt{n}}\omega_{pc}s + 1.2x\omega_{pc}^2}) \\
& \cdot [\frac{0.0988\omega_{pc} \cdot (s^2 + 14.7\omega_{pc}^2)(s^2 + 6.28\omega_{pc}^2)}{(s + 1.36\omega_{pc})(s^2 + 1.75\omega_{pc}s + 2.35\omega_{pc}^2)(s^2 + 0.486\omega_{pc}s + 2.85\omega_{pc}^2)}]. \qquad (12)
\end{aligned}
$$

$$
\begin{aligned}
& H_{tot}(s) \\
& = \frac{0.274x\omega_{pc}^4(s+0.347\omega_{pc})(s^2+14.7\omega_{pc}^2)(s^2+6.28\omega_{pc}^2)}{(s^2+0.347\omega_{pc}s+\omega_{pc}^2)[s^2+1.39(1.25-x)\omega_{pc}s+1.2x\omega_{pc}^2](s+1.36\omega_{pc})(s^2+1.75\omega_{pc}s+2.35\omega_{pc}^2)(s^2+0.486\omega_{pc}s+2.85\omega_{pc}^2)}. \qquad (13)
\end{aligned}
$$

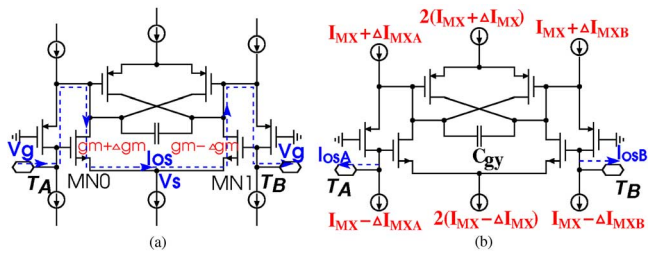

Fig. 9. Mismatch analysis of the FAI. (a) Offset current flowing between $\mathrm{T_A}$ and $\mathrm{T_B}$ results from horizontal mismatch between transistors in the differential pair. [Horizontal mismatch.] (b) Offset currents separately flowing at $\mathrm{T_A}$ and $\mathrm{T_B}$ result from vertical mismatch between the current sources. [Vertical mismatch.]

port TA to port TB even if TA and TB are tied to the same DC voltage V_g. The value and variance of the offset DC current can be derived as

$$I_{os} = \Delta gm(V_g - V_s) \approx \Delta gm U_T ln \frac{I_D}{I_0} \tag{14}$$

where I_0 is the transistor off current when $V_g = V_s = 0$ and is expressed as

$$I_0 = I_{spec} \cdot e^{-V_{th}/nU_T}. \tag{15}$$

V_{th} is the transistor threshold voltage and I_{spec} is the specific current defined as $2\beta nU_T^2$ where β is the transconductance parameter. The ratio between I_D and I_{spec} is the inversion coefficient which is far less than unity in weak inversion [62].

The same analysis can be performed on transistor pair MP and MX, and the total offset currents resulting from horizontal mismatch can be expressed in the following as summation of three transistor pair mismatches:

$$I_{osH} = \Delta gm_{MN} U_T \ln \frac{I_{MX}}{I_{N0}} + \Delta gm_{MX} U_T \ln \frac{I_{MX}}{I_{P0}} + \Delta gm_{MP} U_T \ln \frac{I_{MP}}{I_{P0}}. \tag{16}$$

The vertical mismatch on the other hand refers to the mismatch between the current sources in the upper side and current sinks in the lower side. As shown in Fig. 9(b), the difference between the currents in the upper and lower side will flow out of the FAI through TA and TB. These two offset currents can be written as

$$I_{osVA(B)} = 2\Delta I_{MPA(B)} + 2\Delta I_{MX}. \tag{17}$$

B. Noise

The noise model of the FAI is illustrated in Fig. 10, from which noise current density at the port TA and TB can be derived

$$\overline{i_n^2(\omega)} = g_{MP}^2[\overline{e_{nMP}^2} + \frac{g_{MX}^2 \overline{e_{nMX}^2} + g_{MN}^2 \overline{e_{nMN}^2}}{(g_{MX} - g_{MP})^2 + 4\omega^2 C_{gy}^2}]. \tag{18}$$

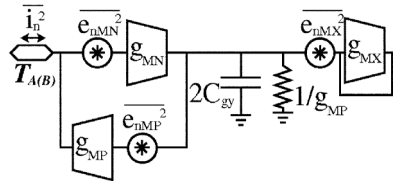

Fig. 10. Noise model of the FAI.

Note that the noise model in Fig. 10 does not include the source degeneration that C_{gy} and MX have on the MP transistor. The actual noise tranconductance for $\overline{e_{nMP}^2}$ is smaller than g_{MP} and thus (18) is in fact the worst-case noise estimation. According to the noise parameters given by the foundry, the transistor noise corner frequency is derived as $\omega_{corner} = 3\pi K_F I_D^{A_F-1}/4qC_{ox}WL$ where K_F and A_F are flicker noise parameters, q is electron charge and C_{ox} is gate oxide capacitance. For the cochlea filter, the biasing current I_D is mapped with the passive center frequency ω_{pc}, and thus we find the point where ω_{pc} equals ω_{corner} as follows:

$$\omega_{pc0} = [\frac{3\pi K_F (3.46U_T C_0)^{A_F-1}}{4qC_{ox}WL}]^{1/2-A_F}. \tag{19}$$

Equation (19) is suitable for PMOS transistor, while for an NMOS transistor WL should be replaced with L^2 according to the noise model provided by the foundry. Besides, parameter A_F is between 1 and 2, and thus the ω_{pc} will be higher than ω_{corner} if it exceeds ω_{pc0}. Therefore a set of values for WL and L^2 which makes ω_{pc0} lower than 20 Hz can be derived so that the passive center frequency of the cochlea filter is always higher than the noise corner frequency and circuit noise is dominated by thermal noise. This setting not only simplifies the following noise calculation but also contributes to better noise performance as the cochlea filter has peak gain at a frequency equal or higher than ω_{pc}. Calculation with the foundry parameters indicates the transistor dimension should meet the requirement that WL is greater than $16 \sim 17\ \mu\mathrm{m}^2$ for PMOS transistors and L^2 is greater than $9 \sim 10\ \mu\mathrm{m}^2$ for NMOS transistors.

Considering only thermal noise, (18) is rewritten and simplified with the cochlear filter parameters as follows:

$$\overline{i_n^2(\omega)} = \frac{8kTI_{STAT}}{3U_T}[1 + \frac{2x}{(x-1.25)^2 + 0.521(\frac{\omega}{\omega_{pc}})^2}]. \tag{20}$$

C. Comprehensive Analysis

Based on the analysis above, a more complete FAI model with mismatch and noise considerations is derived and illustrated in Fig. 11. The DC offset currents affect the DC operation point of circuits and thus as shown in Fig. 4, at least one port of each FAIs is connected to low impedance source to release the offset currents. In the BPF and LPF, all FAIs have one port shorted to ground (BPF) or FDDA buffer output (LPF), releasing I_{osH} and one branch of I_{osV}. The remaining branch of I_{osV} flows through the FAI and causes a DC shift of $I_{osV} \cdot R_{FAI}$ which is in the worst case less than 1mV if the variances of parameters do not exceed 1%. FAIs in the elliptic filter should

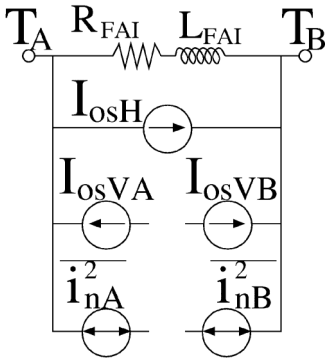

Fig. 11. FAI model with offsets and noise currents.

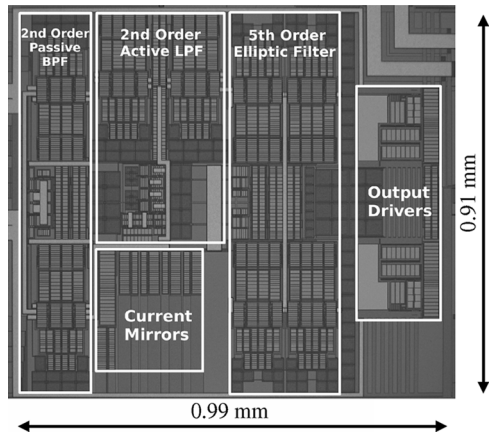

Fig. 12. Chip micrograph showing the cochlea filter channel.

be analyzed separately. The FAI2s have one port connected to the OTA followers while the FAI4s have one port connected to the other port of FAI2s. Thus I_{osH} and I_{osV} of both FAI2 and FAI4 flow through the OTA follower and cause DC shift of $(I_{osH}+2I_{osV})nU_T/I_{STAT}$ which is in the worst less than 40 mV if the variances of parameters do not exceed 1%. Besides, the offset currents in FAI4 flow through FAI2 in addition to one branch of I_{osV} of FAI2 itself and cause DC shift of $(I_{osH}+3I_{osV})R_{FAI2}$ which is in the worst case less than 3 mV if the variances of parameters do not exceed 1%. In the end, one branch of I_{osV} flows through FAI4 and causes DC shift of $I_{osV}R_{FAI4}$ which is less than 0.1 mV if the variances of parameters do not exceed 1%. Simulations prove the above-mentioned level of DC shift has insignificant effects on the circuit operation. Thus by referring to the parameter matching equations provided by the foundry, the width and length of the transistors in the FAIs are optimized so that the probability of the parameter variance being greater than 1% is limited to 1%.

Taking into consideration the parameter matching, the noise corner frequency setting explained in the previous section and also the weak inversion requirement, the dimensions of the transistor pairs in FAI are set to $W = 180\ \mu\mathrm{m}$ and $L = 3.5\ \mu\mathrm{m}$ for PMOS pairs MP and MX while $W = 100\ \mu\mathrm{m}$ and $L = 3.5\ \mu\mathrm{m}$ for NMOS pair MN.

For the noise analysis, the input referred noise of the BPF and LPF in the cochlea filter can be derived as following:

$$\overline{V_{niBPF}^2(\omega)} = 0.0651 \cdot \frac{\overline{i_{nBPF}^2(\omega)}}{\omega_{pc}^2 C_0^2} \tag{21}$$

$$\overline{V_{niLPF}^2(\omega)} = \frac{2\overline{i_{nLPF}^2(\omega)}}{x^2\omega_{pc}^2 C_0^2}[\frac{0.174\omega^2}{\omega_{pc}^2} + 0.333(1.25-x)^2]. \tag{22}$$

Noise calculation for the elliptic filter is far more complicated, but as the BPF and LPF provide all the gain for the cochlea filter, the noise from the elliptic filter is less significant compared with BPF and LPF when referred to the input. Therefore, neglecting the noise from elliptic filter, input referred noise density of the cochlea filter channel is the sum of BPF input referred noise and LPF input referred noise divided by gain of BPF and can be written as (23), at the bottom of the page, combining (4), (20), (21) and (22) and using ξ to represent ω/ω_{pc}. As explained above, cochlea filter bandwidth has been set as $\sqrt{2}\omega_{pc}$, and thus integrated input referred noise of the cochlea filter is calculated as follows:

$$\begin{aligned} V_{inoise}^2 &= \int_0^{\sqrt{2}} \overline{V_{ni}^2(\xi)}d\xi \\ &= \frac{440kT}{\omega_{pc}C_0}[(\frac{1}{x}-\frac{1}{6})^2 + 0.65]. \end{aligned} \tag{24}$$

Equations (24) indicates that the filter input-referred noise decreases with increasing center frequency and tuning factor. A cochlea filter with passive center frequency of 100 Hz has 47 $\mu\mathrm{V_{rms}}$ input noise in the low Q mode ($x = 0.75$) and 27 $\mu\mathrm{V_{rms}}$ in the high Q mode ($x = 1.24$).

V. Results

Based on the design explained above, a cochlea filter channel has been fabricated using AMS 0.35 μm 2-poly 4-metal process, as shown in Fig. 12. A prototype PCB and an NI PXI platform are built to characterize the filter, as illustrated in Fig. 13.

$$\begin{aligned} &\overline{V_{ni}^2(\xi)} \\ &= \frac{1.15kT}{\omega_{pc}C_0}\{\frac{[(1.25-x)^2+2x+0.521\xi^2](\xi^4-1.86\xi^2+1)}{x^2(\xi^2+0.14)} + 0.521 + \frac{2}{0.12+\xi}\} \end{aligned} \tag{23}$$

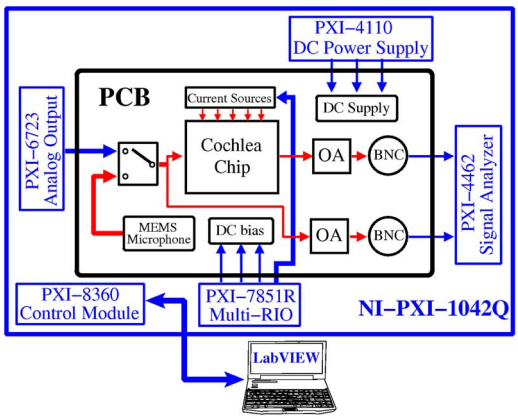

Fig. 13. Block diagram of the experimental setup. Input to the cochlea filter chip can be switched between the PXI-6723 analog output module and a MEMS microphone (ADMP401). Biasing currents that set the operating condition of the cochlea filters are controlled by the PXI-7851R multi-function reconfigurable IO module. The output of the cochlea filters are further amplified by an off-chip amplifier (OA) and interfaced with the PXI-4462 dynamic signal analyzer through BNC connectors.

The static current of the cochlea filter I_{STAT} is set with different values from 37.14 pA to 9.915 nA so as to make the filter operate in nine frequency regions corresponding to the octave audio bands from 31 Hz to 8 kHz. The BPF current I_{BPF} is set where ω_{pc} is approximately $10 \sim 20\%$ smaller than the corresponding octave frequency value. The LPF current I_{LPF} is tuned in the region from where the LPF center frequency overlays with ω_{pc} (LQ mode), to where the LPF peak gain is maximized (HQ mode). The elliptic filter current I_{ELLI} is set as $1.2I_{STAT}$ as explained in Section III.

A. Frequency Response

1) Magnitude Response: Frequency responses of the nine filter bands in magnitude are measured and plotted in Fig. 14. Apart from the LQ and HQ modes mentioned above, responses of the cochlea filters in medium Q (MQ) mode are also measured, where I_{LPF} is adjusted so that center frequency (CF) of the entire filter is located approximately at the corresponding octave frequency value. As shown in Fig. 14, the passive and gentle low-frequency band, active and selective mid-band and steep roll-off are achieved in all of the filters. Although a 40dB of peak gain variation range has been measured from chinchilla cochlea [16], [18], more physiological measurements in recent years report approximately $20 \sim 30$ dB of gain variation [17], [19]–[21], [23]. The high-frequency amplitude plateau in biological cochlea [28] is also found in the 31 Hz, 63 Hz, 125 Hz, 500 Hz, 1 kHz and 2 kHz bands. Besides, it is observed that CFs of LQ mode locate approximately $10 \sim 20\%$ leftwards from the CFs of MQ, while CFs of HQ mode locate $10 \sim 20\%$ rightwards. In other words, the CFs become higher together with increasing peak gain and selectivity, which agrees with biological cochlea behavior [16]–[21]. The detailed results are listed in Table I. Noticing that as parasitic resistance of wires exists in real VLSI implementation, the range of tuning factor x in Table I is wider than the value used in previous section $(0.75 \sim 1.24)$. To improve the precision of current measurement, current mirrors with 1:100 ratio are used on chip. Therefore, the actually measured off-chip currents are 100 times as much as those values in Table I.

2) Phase Response: As both biological cochlea and the proposed filter have minimum-phase property, their phase responses should also be similar when the magnitude responses are matched. The phase responses of the 31 Hz and 8 kHz bands are illustrated in Fig. 15. As also observed in the physiological results, the filter phase lag increases with frequency in the pass-band [16]–[19], [21], [23]. The LQ phase lag at the passive centre frequency is slightly over half cycle [17], [18], [20], [21], while the HQ phase lag at the active centre frequency is approximately one cycle [17], [21]–[23]. The LQ response has more phase lag at frequencies lower than ω_{ac} (active center frequency) while the HQ response has more phase lag at frequencies higher than ω_{ac} [17]–[21].

3) Group Delay: Fig. 15 indicates that the group delay reaches maximum at ω_{ac} where the phase response curve has steepest slope. Fig. 16 shows the maximum group delay in unit of periods across different center frequencies. As expected, the group delay increases from LQ to HQ mode. The maximum group delays in LQ and MQ modes are approximately 5 periods while the maximum group delay in HQ mode is in the region of 10 periods. Fig. 17 shows the physiologically measured maximum group delay in human cochlea [64]. The measurement in [64] is based on the stimulus-frequency emission method which stimulates the cochlea with low-intensity input. Therefore the results in [64] correspond to the HQ response in this work. The comparison in Fig. 17 shows the cochlea filter has similar order of group delay with human cochlea.

B. Time Domain Response

Impulse responses of the cochlea filter in 31 Hz and 8 kHz bands are given in Fig. 18, combined with response from BPF, LPF and elliptic filter separately. As the cochlea filter is a composite of three filters in cascade, its overall impulse response is the convolution of three individual responses. From Fig. 18, it is observed that for HQ mode, envelopes of response are not smooth and there is a trough near the third ringing crests, while for LQ mode, however, the envelopes are fairly smooth. The reason for this phenomenon is that, as shown in the decomposed response plots, BPF and elliptic filters settle much quicker than LPF in HQ mode, and thus although their responses are significant enough to affect the convolved overall response in the early stage, after 100 ms in Fig. 18(a) and 0.4 ms in Fig. 18(b), the overall responses are fully dominated by LPF. Therefore the impulse responses appear to have two stages of behavior, the convoluted response and the LPF-dominant response, separated by the settling of BPF and elliptic filter. As for the LQ mode, the LPF settles even faster than the BPF and elliptic filter, and thus the overall responses are smooth over time.

The post-dominance of LPF in HQ mode results in a shift of ringing frequency. As shown in Fig. 18, initial ringing periods in convolved responses (t_{d1}) are wider than ringing periods in the LPF-dominant responses (t_{d2}). This effect agrees with the frequency gliding phenomenon observed in physiological measurements, where instantaneous frequency of biological cochlea response to clicks is not constant but increases over time until

TABLE I
FREQUENCY RESPONSE SPECIFICATIONS OF COCHLEA FILTER IN DIFFERENT CONFIGURATIONS

		CF *	CF Variation	GD *	ERB *	I_{STAT}	x	PG *	PG Variation	Q factor	Roll-off Slope
Filter1	LQ	25Hz	-19.3% ∼+12.9%	132ms	14.3Hz	37.14pA	0.68	7.736dB	18.8dB	2.08	125.5dB/dec
	MQ	31Hz		126ms	14.8Hz		1.07	12.48dB		3.16	189.3dB/dec
	HQ	35Hz		396ms	3.97Hz		1.39	26.53dB		15.9	336.2dB/dec
Filter2	LQ	53Hz	-15.9% ∼+17.5%	53.9ms	32.5Hz	78.41pA	0.68	8.787dB	20.4dB	2.11	110.8dB/dec
	MQ	63Hz		63.5ms	27.5Hz		0.95	14.26dB		3.28	159.2dB/dec
	HQ	74Hz		168ms	7.87Hz		1.45	29.14dB		19.5	274.2dB/dec
Filter3	LQ	105Hz	-16% ∼+12%	32.8ms	54.3Hz	143.7pA	0.82	9.971dB	21.5dB	2.28	124.1dB/dec
	MQ	125Hz		35.1ms	41.8Hz		1.26	19.07dB		3.79	183.9dB/dec
	HQ	140Hz		73.6ms	11.0Hz		1.48	31.51dB		19.4	301.8dB/dec
Filter4	LQ	220Hz	-12% ∼+10%	16.3ms	106Hz	279.1pA	0.92	11.52dB	20.6dB	2.44	132.4dB/dec
	MQ	250Hz		16.8ms	88.1Hz		1.23	17.72dB		3.57	172.4dB/dec
	HQ	275Hz		33.1ms	24.6Hz		1.53	32.10dB		15.3	290.9dB/dec
Filter5	LQ	430Hz	-12.2% ∼+11.2%	10.6ms	203Hz	554.0pA	0.88	13.14dB	20.5dB	2.69	110.6dB/dec
	MQ	490Hz		11.4ms	162Hz		1.26	21.32dB		4.26	161.9dB/dec
	HQ	545Hz		17.4ms	53.4Hz		1.55	33.64dB		14.0	240.5dB/dec
Filter6	LQ	0.9kHz	-14.3% ∼+14.3%	4.03ms	484Hz	1.189nA	0.89	10.79dB	21.3dB	2.20	116.3dB/dec
	MQ	1.05kHz		4.82ms	386Hz		1.24	17.74dB		3.00	160.9dB/dec
	HQ	1.2kHz		7.65ms	101Hz		1.55	32.07dB		16.0	391.4dB/dec
Filter7	LQ	1.7kHz	-15% ∼+10.8%	1.36ms	0.864kHz	2.156nA	0.88	12.23dB	20.0dB	2.62	114.6dB/dec
	MQ	2kHz		1.47ms	0.629kHz		1.31	21.38dB		3.64	166.8dB/dec
	HQ	2.2kHz		4.04ms	0.238kHz		1.54	32.22dB		14.7	238.5dB/dec
Filter8	LQ	3.5kHz	-10.3% ∼+12.8%	706μs	1.69kHz	4.291nA	0.91	11.28dB	20.0dB	2.76	120.7dB/dec
	MQ	3.9kHz		950μs	1.33kHz		1.29	18.95dB		3.71	160.6dB/dec
	HQ	4.4kHz		2.04ms	0.375kHz		1.55	31.26dB		18.3	272.1dB/dec
Filter9	LQ	7.1kHz	-14.5% ∼+10.8%	223μs	4.01kHz	9.915nA	0.68	8.152dB	21.1dB	2.25	123.6dB/dec
	MQ	8.3kHz		369μs	2.94kHz		1.20	19.03dB		3.32	176.0dB/dec
	HQ	9.2kHz		1.24ms	1.28kHz		1.55	29.23dB		10.6	268.4dB/dec

*CF = Center Frequency; GD = Group Delay; ERB = Equivalent Rectangular Bandwidth; PG = Peak Gain.

settled at steady state [24]–[27]. The gliding phenomenon is a standard for cochlea model evaluation suggested by the physiologists [24], [26]. Its origin has been proved to be independent of the nonlinear active process [24], [26]. Similarly, the frequency shift in this cochlea filter is not based any active control and thus provide a basis for future research on how the gliding effects influence signal processing in the cochlea.

C. Noise Measurement

Output noise spectrum from the 31 Hz and 8 kHz bands, with comparison between LQ, MQ and HQ modes are illustrated in Fig. 19. The 50 Hz harmonics shown are due to the ripples of power supply. Besides, the noise spectrum of the HQ mode of 8 kHz band has prominent peaks at CF harmonics. This indicates that the 8 kHz band has more harmonic distortion than the 31 Hz band especially in the HQ mode. As shown in Table I, the DC current in FAI scales with CF. Therefore, the operation of transistors in the FAI moves from weak inversion towards moderate inversion when the center frequency increases. However, the DC operating points of the filter are designed based on the weak inversion assumption, and the circuit linearity will be affected by the DC variation. The CF harmonics should be theoretically well attenuated by the elliptic filter. However, the transistor in moderate inversion has lower gm/I_D compared with weak inversion which makes the FAI inductance deviate from designed values and consequently degrade the elliptic filter performance. The harmonic distortion issue will be discussed further in Section V-D.

The input-referred noise density at the center frequency of the 9 filter bands in LQ, MQ and HQ modes are illustrated in Fig. 20. Compared with noise predication function of (24), the measured results in MQ and HQ modes agree in terms of the fact that input referred noise decreases for higher center frequencies. However, LQ mode shows noise does not vary much from low to high frequencies, because the filter selectivity is not high enough to overcome the added power supply harmonics from the increase of filter bandwidth. Besides, Fig. 20 also proves the increase of tuning factor x results in lower input referred noise except the 31 Hz band where MQ has even wider equivalent rectangular bandwidth than LQ mode as shown in Table I.

D. Distortion Measurement

1) Total Harmonic Distortion (THD) and Signal-to-Noise-and Distortion Ratio(SINAD): Fig. 21 shows the plots of THD and SINAD against input level based on the measured results from the 31 Hz and 8 kHz bands. The SINAD of both filters generally maintain above the 12 dB SINAD threshold for intelligent hearing before THD reaches the edge of 5% limit. The HQ mode has most significant harmonic distortion due to high LPF gain and thus high signal amplitude at the elliptic filter input. As predicted in the noise spectrum [Fig. 19(b)], the 8 kHz band has more harmonic distortion than the 31 Hz band. Based on the 5% THD limit, the maximum input level is plotted against filter center frequencies, so is the maximum SINAD. Fig. 22 shows the filter linearity tends to degrade with higher frequencies.

2) Two-Tone Inter-Modulation Distortion: Inter-modulation distortion test is performed and the results are shown in Fig. 23. The third-order inter-modulation product $2f_1 - f_2$ appears to be the most prominent distortion component because it is designed to coincide with the filter center frequency. The inter-modulation distortion is also found in the biological cochlea, which

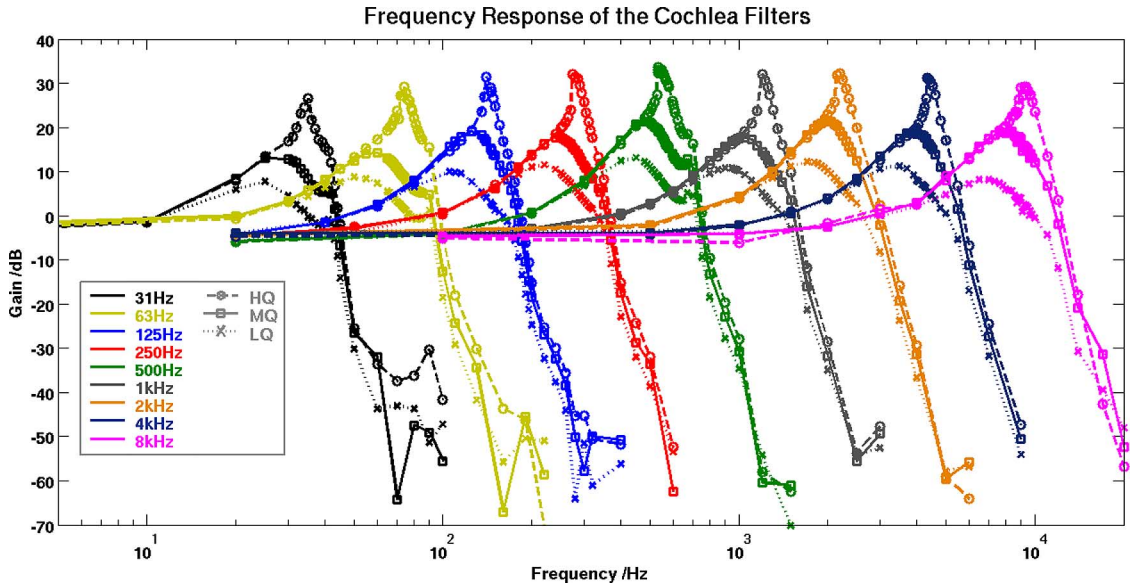

Fig. 14. Measured frequency responses of 9 cochlea filters covering octave audio bands from 31 Hz to 8 kHz. The LQ, MQ and HQ modes respectively correspond to the biological response with high, normal and low intensity sound stimulus. Tuning of the filter from LQ to HQ is achieved by adjusting only one circuit parameter (I_{LPF}).

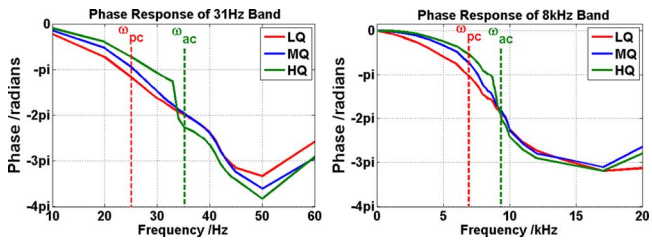

Fig. 15. Measured phase response of the 31 Hz band and 8 kHz band.

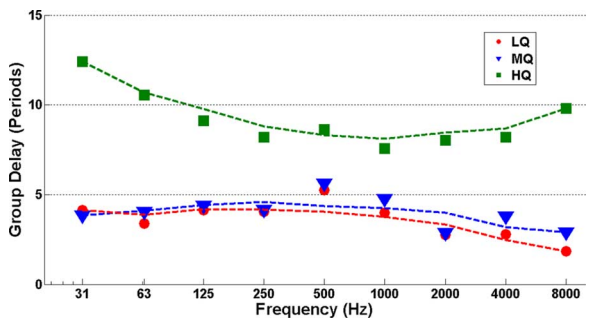

Fig. 16. Measured maximum group delay across different center frequencies.

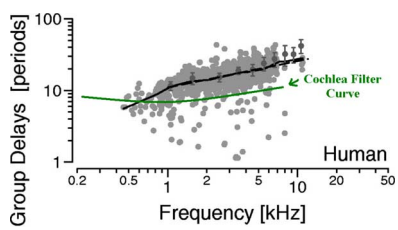

Fig. 17. The HQ maximum group delay curve in comparison with physiologically measured results from human cochlea. The figure is adapted from the Fig. 5 in [64].

proves that the biological hearing system can tolerate 17 $\sim$ 24 dB worst-case spurious free dynamic range (SFDR) [28]. Fig. 24 plots the filter maximum input range measured using the 17 dB SFDR limit. It shows in most frequency bands the maximum input range is further reduced compared with the results based on the 5% THD limit. Nevertheless, the input range of the 8 kHz band appears even higher than the results in Fig. 22 and there is no significant degradation compared with the other bands. The distortion products of interest in the inter-modulation measurement are in-band signals while the CF harmonics measured in the THD test are out-of-band signals. Therefore, the high harmonic distortion measured in the 8 kHz band is probably due to the degraded stop-band attenuation.

E. Critical Bandwidth

An equivalent rectangular band-pass filter model is illustrated in Fig. 25, which helps us to understand the critical band and frequency discrimination feature of the designed cochlea filters. The calculated equivalent rectangular bandwidth (ERB) and measured -3 dB bandwidth of the cochlea filters are plotted versus corresponding CF in Fig. 26, together with the approximated bandwidth of human auditory filters derived from the formula given by Glasberg and Moore [65] for comparison. It shows that -3 dB bandwidth is generally narrower than the ERB, but their discrepancy is not significant. The exact bandwidth values are listed in Table I. We observe from Fig. 26 that the ERB curve given by Glasberg and Moore from psycho-acoustical research lies in-between the ERB curves of the MQ and HQ modes. However as the cochlea filter can be continuously tuned, it is possible to find a condition between the MQ and HQ modes where the ERB versus CF curve corresponds with better agreement to psycho-acoustical results [65].

F. Testing With Acoustic Signals

A segment of acoustic signal (mixed sounds from musical instruments of the horn and bass drum) is applied to the cochlea

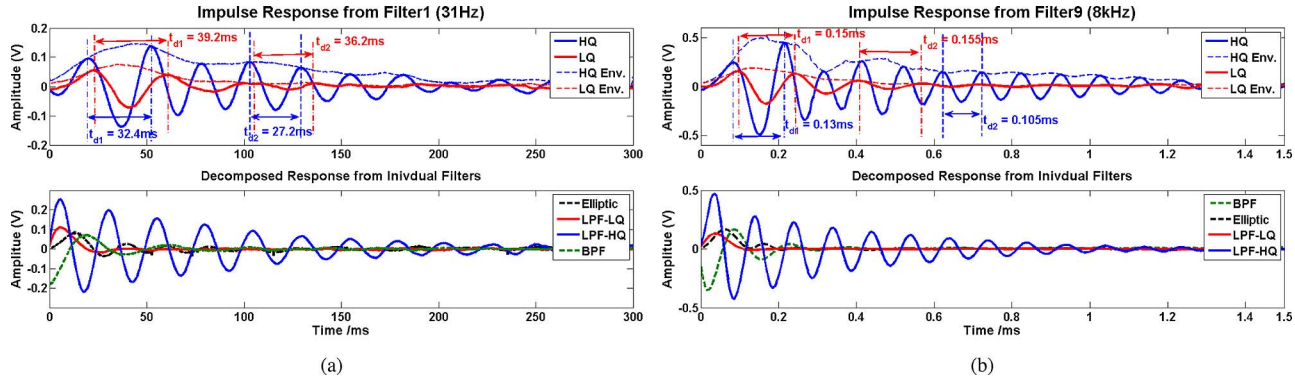

(a) (b)

Fig. 18. Measured impulse response from (a) 31 Hz and (b) 8 kHz band cochlea filters. The decrease of ringing period (t_d) with time agrees with the gliding phenomenon in biological cochlea.

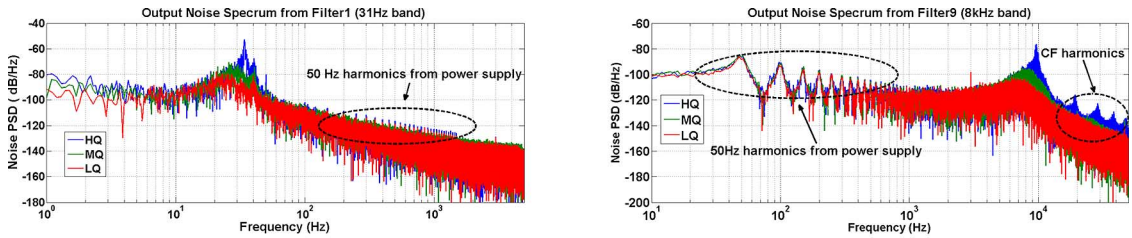

(a) (b)

Fig. 19. Measured output noise spectrum from (a) 31 Hz and (b) 8 kHz band filters. Like the frequency response shown in Fig. 14, the spectrum shape has stable low-frequency band (does not vary with tuning), tunable mid-frequency band and steep roll-off at stop-band.

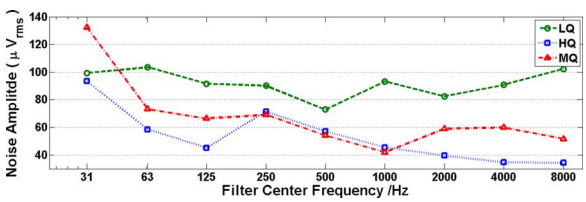

Fig. 20. Plot of measured integrated input-referred noise versus center frequency.

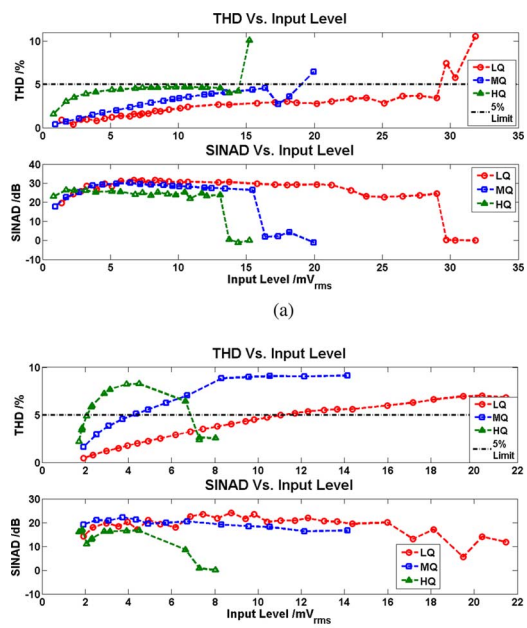

Fig. 21. Measured THD and SINAD plots versus input level from (a) 31 Hz and (b) 8 kHz band filters. The 5% THD limit is suggested for auditory circuits [48].

filter. As the frequencies around 63 Hz, 1 kHz and 2 kHz have highest intensity, the cochlea filter is tested in these three frequency bands accordingly and the results are shown in Fig. 27. It is notable that, the noise around center frequency is selectively amplified rather than the signal in the HQ output of the 1 kHz band, as the cochlea filter currently does not have the capability to distinguish between signal and noise. This problem can be potentially solved with the addition of an SNR estimation mechanism [66]. Also, the results show that the octave distribution of filter center frequencies is inadequate for high performance auditory processing task. The purpose of using octave distribution in this paper is only to prove the frequency range that the cochlea filter covers. As for future applications, more sophisticated distributions like one third octave or bark scale will be investigated.

G. Summary

Table II summarizes the measured specifications of the cochlea filter chip. Note that the power dissipation of the FDDA and the output buffers does not scale with filter center frequency. Consequently, the power dissipation of the 31 Hz filter is only one-third less than that of the 8 kHz filter. Table III gives scores in terms of auditory filter model following the criteria given by Lyon [67]. Noticing that the current cochlea filter has not been integrated with automatic-Q-control (AQC) mechanism, but as the measured results indicate the filter can

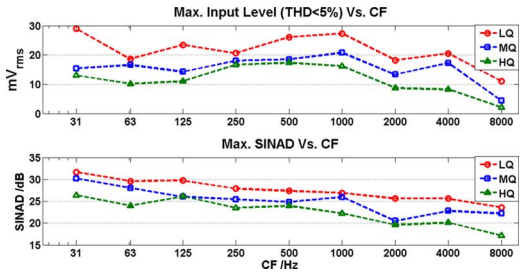

Fig. 22. Measured maximum input range and SINAD across different center frequencies.

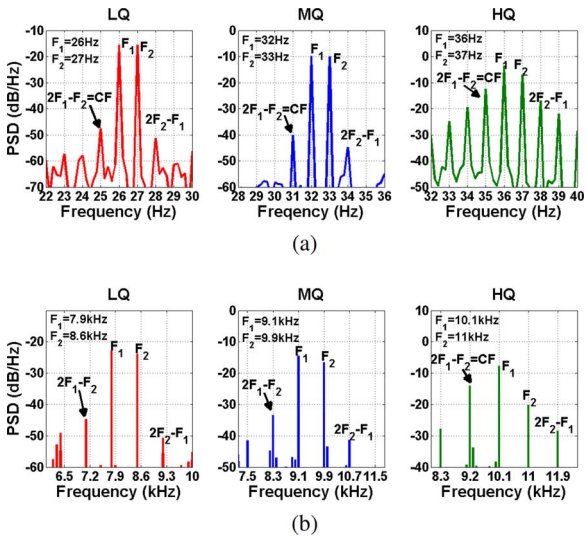

Fig. 23. Two-tone inter-modulation distortion measured from (a) 31 Hz and (b) 8 kHz band filters. Two signals in equal amplitude (10 mV) with primary frequencies f_1 and f_2 such that $2f_1 - f_2 = \mathrm{CF}$ are applied to the cochlea filter.

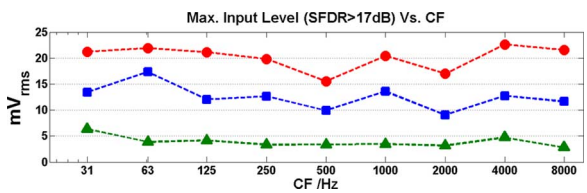

Fig. 24. Maximum input range measured across different center frequencies using the 17dB SFDR limit.

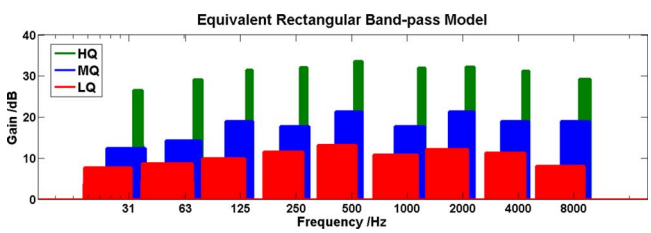

Fig. 25. Equivalent rectangular band-pass filter model of the cochlea filters. The rectangular filters pass the equal amount of energy with the corresponding cochlea filters in Fig. 14.

be actively tuned according to sound level, a potential '+' credit is given in the 'dynamic' criterion.

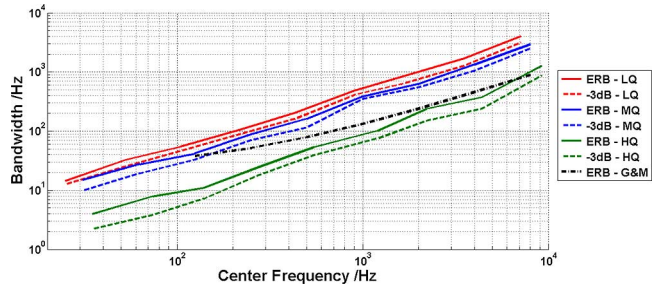

Fig. 26. ERB and −3 dB bandwidth of the cochlea filters in comparison with approximated ERB of human auditory filters [65].

VI. Conclusion

Design and experimental results of a bio-realistic analog cochlea filter have been presented, the highlights of which can be summarized as following:

- The filter is highly faithful with measured response from physiological experiment on mammalian cochlea, with passive and gentle response in low-frequency band, active and selective response in mid-band and a sharp transition from pass-band into stop-band. Besides, similarity of the filter in phase response and impulse response has also been demonstrated.
- The filter can operate at center frequencies from as low as 31 Hz to 8 kHz. Experimental results show that the operation in deep low frequency is even more robust than in high frequencies.
- Filter efficiency has been improved by the specialized triple-stage design, to the extent that:
  - The active behavior observed in biology is emulated by tuning only one circuit parameter (tuning factor x), and positions of only one pair of poles (poles of LPF) are shifted in tuning. The reduced tuning complexity will prospectively increase the robustness and dynamic performance of the proposed cochlea system in Fig. 1.
  - In previous second-order section based filters, the bio-realistic 330 dB/dec roll-off requires the filter order to be at least 16 [68]. The same steepness is achieved in our 9^{th} order design by using a sharp cut-off elliptic filter. The lower filter order leads to less power consumption and smaller chip area for each channel, and thus a larger number of channels can be implemented in a parallel filter bank, which will prospectively increase the functionality of the cochlea system shown in Fig. 1.

On the other hand, additional improvement and future work are still necessary including:

- The filter dynamic range is constrained by the limited linear range of the tanh transconductance in FAIs. Linearisation techniques such as multi-tanh [69] may be investigated in the future.
- Filter array with center frequencies distributed in more applicable manner such as one-third octave or bark scale should be implemented so as to fulfill practical auditory processing tasks.
- Other mechanisms including local control (AQC) and signal-noise distinguishing will be integrated with the

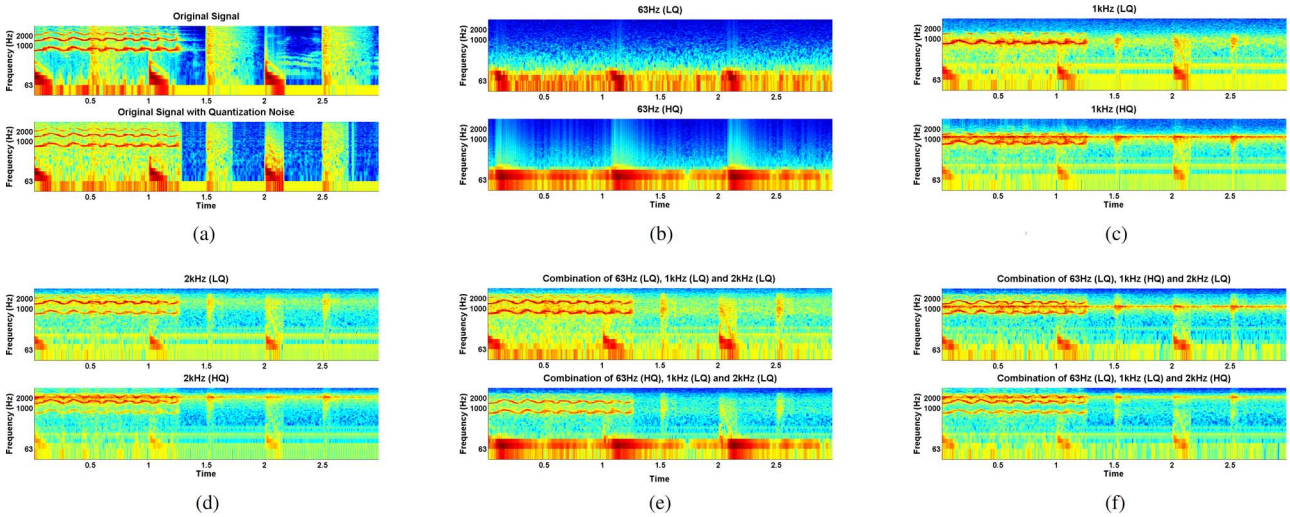

Fig. 27. Measured time-frequency spectrogram of outputs from cochlea filters in response to mixed signals of the horn and bass drum. The signal is applied together with quantization noise from the 13-bit DAC in NI-6732 analog output. Outputs from the three bands and their combinations prove the frequency selectivity of the cochlea filters. Also, the quantization noise has been attenuated, especially by the filter in HQ mode. (a) Input signals. (b) Output from 63Hz filter. (c) Output from 1 kHz filter. (d) Output from 2 kHz filter. (e) Combination of the three filter outputs. (f) Combination of the three filter outputs.

TABLE II
SUMMARY OF CHIP SPECIFICATIONS

Fabrication process	AMS 0.35 μm 3.3V 2P4M
Channel area	$0.9mm^2$ (0.99mm X 0.91mm)
Center frequency	31Hz∼8kHz
Power dissipation	59.5μW @31Hz; 90.0μW @8kHz.
Peak gain variation	18.8dB @31Hz; 21.1dB @8kHz.
Cut-off slope	125.5dB/dec(LQ) ∼ 336.2dB/dec(HQ) @31Hz; 123.6dB/dec(LQ) ∼ 268.4dB/dec(HQ) @8kHz.
Phase delay @CF	210.5degree(LQ) ∼ 373.1degree(HQ) @31Hz; 204.8degree(LQ) ∼ 347.4degree(HQ) @8kHz.
Min. input noise	93.34μV_{rms} @31Hz; 34.32μV_{rms} @8kHZ.
Max. input swing (THD$<5\%$)	82.0 mV_{p-p} @31Hz; 31.2 mV_{p-p} @8kHz.
Max. input swing (SFDR>17dB))	60 mV_{p-p} @31Hz; 61 mV_{p-p} @8kHz.
SINAD	26.38dB (HQ) ∼ 31.67dB (LQ) @31Hz; 17.13dB (HQ) ∼ 23.56dB (LQ) @8kHz.
Expected dynamic range with AQC *	49.8dB @31Hz; 50.2dB @8kHz.

*The lower bound is determined by the HQ input-referred noise and the upper bound is determined by the LQ linear range.

TABLE III
SCORES AS AUDITORY FILTER MODEL [67]

1. Simple	Laplace domain	6. Stable tail	+
2. BW control	+	7. Runnable	+
3. Peak/skirts	+	8. Waves	-
4. Asymmetry	+	9. Impulse resp.	+
5. Gain Variation	+	10. Dynamic	+ (potentially)

filter and ultimately a system illustrated in Fig. 1 will be implemented.

ACKNOWLEDGMENT

The authors would like thank Mr. T. Chen for his help in taking the chip micrograph.

REFERENCES

[1] W. S. Rhode, "Some observations on cochlear mechanics," *J. Acoust. Soc. Amer.*, vol. 64, no. 1, pp. 158–176, Jul. 1978.
[2] B. S. Wilson and M. F. Dorman, "Interfacing sensors with the nervous system: lessons from the development and success of the cochlear implant," *IEEE Sensors J.*, vol. 8, no. 1, pp. 131–147, Jan. 2008.
[3] K. H. Kim, S. J. Choi, J. H. Kim, and D. H. Kim, "An improved speech processing strategy for cochlear implants based on an active nonlinear filterbank model of the biological cochlea," *IEEE Trans. Biomed. Circuits Syst.*, vol. 56, no. 3, pp. 828–836, Mar. 2009.
[4] T. Harczos, A. Chilian, and P. Husar, "Making use of auditory models for better mimicking of normal hearing processes with cochlear implants: the SAM coding strategy," *IEEE Trans. Biomed. Circuits Syst.*, vol. 7, no. 4, pp. 414–425, Aug. 2013.
[5] Z. Tuske, P. Golik, R. Schluter, and F. R. Drepper, "Non-stationary feature extraction for automatic speech recognition," in *Proc. Int. Conf. Acoustics, Speech and Signal Processing*, 2011, pp. 5204–5207.
[6] M. J. Newton and L. S. Smith, "A neurally inspired musical instrument classification system based upon the sound onset," *J. Acoust. Soc. Amer.*, vol. 131, no. 6, pp. 4785–4798, Jun. 2012.
[7] X. Valero and F. Alias, "Gammatone cepstral coefficients: biologically inspired features for non-speech audio classification," *IEEE Trans. Multimedia*, vol. 14, no. 6, pp. 1684–1689, Dec. 2012.
[8] X. Zhao, Y. Shao, and D. Wang, "CASA-based robust speaker identification," *IEEE Audio, Speech, Language Process.*, vol. 20, no. 5, pp. 1608–1616, Feb. 2012.
[9] B. Gao, W. L. Woo, and S. S. Dlay, "Unsupervised single-channel separation of nonstationary signals using gammatone filterbank and itakura-saito nonnegative matrix two-dimensional factorizations," *IEEE Trans. Circuits Syst. I, Reg. Papers*, vol. 60, no. 3, pp. 662–675, Mar. 2013.
[10] J. Qi, D. Wang, Y. Jiang, and R. Liu, "Auditory features based on gammatone filters for robust speech recognition," in *Proc. IEEE Int. Symp. Circuits and Syst.*, 2013, pp. 305–308.
[11] S. Mandal, S. M. Zhak, and R. Sarpeshkar, "A bio-inspired active radio-frequency silicon cochlea," *IEEE. J. Solid-State Circuits*, vol. 44, no. 6, pp. 1814–1828, Jun. 2009.
[12] C. J. Galbraith, R. D. White, L. Cheng, K. Grosh, and G. M. Rebeiz, "Cochlea-based RF channelizing filters," *IEEE Trans. Circuits Syst. I, Reg. Papers*, vol. 55, no. 4, pp. 969–979, May 2008.
[13] R. Sarpeshkar, *Ultra Low Power Bioelectronics: Fundamentals, Biomedical Applications, and Bio-Inspired Systems*. Cambridge, U.K.: Cambridge Univ. Press, 2011, pp. 9–14.
[14] L. Gouveia, T. J. Koickal, and A. Hamilton, "An asynchronous spike-event coding scheme for programmable analog array," *IEEE Trans. Circuits Syst. I, Reg. Papers*, vol. 58, no. 4, pp. 791–799, Apr. 2011.

[15] G. Sanchez, T. J. Koickal, A. Sripad, L. C. Gouveia, A. Hamilton, and J. Madrenas, "Spike-based analog-digital neuromorphic information processing system for sensor applications," in *Proc. IEEE Int. Symp. Circuits and Syst.*, 2013, pp. 1624–1627.

[16] M. A. Ruggero, S. S. Narayan, A. N. Temchin, and A. Recio, "Mechanical bases of frequency tuning and neural excitation at the base of the cochlea: Comparison of basilar-membrane vibrations and auditory-nerve-fiber responses in chinchilla," *Proc. Nat. Acad. Sci. USA*, vol. 97, no. 22, pp. 11744–11750, Oct. 2000.

[17] T. Ren and A. L. Nuttall, "Basilar membrane vibration in the basal turn of the sensitive gerbil," *Hear. Res.*, vol. 151, no. 1-2, pp. 48–60, Jan. 2001.

[18] W. S. Rhode, "Basilar membrane mechanics in the 6-9 kHz region of sensitive chinchilla cochleae," *J. Acoust. Soc. Amer.*, vol. 121, no. 5, pp. 2792–2804, May 2007.

[19] A. R. -Spinoso, S. S. Narayan, and M. A. Ruggero, "Basilar membrane responses to noise at a basal site of the chinchilla cochlea: quasi-linear filtering," *J. Assoc. Res. Otolaryngol*, vol. 10, no. 4, pp. 471–484, Dec. 2009.

[20] F. Chen, D. Zha, A. Fridberger, J. Zheng, N. Choudhurry, S. L. Jacques, R. K. Wang, X. Shi, and A. L. Nuttall, "A differentially amplified motion in the ear for near-threshold sound detection," *Nat. Neurosci.*, vol. 14, no. 6, pp. 770–774, Jun. 2011.

[21] C. P. Versteegh and M. v. d. Heijden, "Basilar membrane responses to tones and tone complexes: nonlinear effects of stimulus intensity," *J. Assoc. Res. Otolaryngol.*, vol. 13, no. 6, pp. 785–798, Dec. 2012.

[22] A. N. Temchin, A. R. -Spinoso, H. Cai, and M. A. Ruggero, "Traveling waves on the organ of Corti of the chinchilla cochlea: spatial trajectories of inner hair cell depolarization inferred from responses of auditory-nerve fibers," *J. Neurosci.*, vol. 32, no. 31, pp. 10522–10529, Aug. 2012.

[23] W. He and T. Ren, "Basilar membrane vibration is not involved in the reverse propagation of otoacoustic emissions," *Sci. Rep.*, vol. 3, doi: 10.1038/sre01874.

[24] E. d. Boer and A. L. Nuttal, "The mechanical waveform of the basilar membrane. I. frequency modulations (glides) in impulse responses and cross-correlation functions," *J. Acoust. Soc. Amer.*, vol. 101, no. 6, pp. 3583–3592, Jun. 1997.

[25] A. Recio and W. S. Rhode, "Basilar membrane responses to broadband stimuli," *J. Acoust. Soc. Amer.*, vol. 108, no. 5, pp. 2281–2298, Nov. 2000.

[26] C. A. Shera, "Frequency glides in click responses of the basilar membrane and auditory nerve: their scaling bahavior and origin in traveling-wave dispersion," *J. Acoust. Soc. Amer.*, vol. 109, no. 5, pp. 2023–2034, May 2001.

[27] A. N. Temchin and A. R. -Spinoso, "Timing of cochlear responses inferred from frequency-threshold tuning curves of auditory-nerve fibers," *Hear. Res.*, vol. 272, no. 1-2, pp. 178–186, Feb. 2011.

[28] L. Robles, M. A. Ruggero, and N. C. Rich, "Two-tone distortion in the basilar membrane of the cochlea," *Nature*, vol. 349, pp. 413–414, Jan. 1991.

[29] R. F. Lyon and C. Mead, "An analog electronic cochlea," *IEEE Trans. Acoust. Speech Signal Process.*, vol. 36, no. 7, pp. 1119–1134, Jul. 1988.

[30] L. Watts, A. Kerns, R. F. Lyon, and C. Mead, "Improved implementation of the silicon cochlea," *IEEE J. Solid-State Circuits*, vol. 27, no. 5, pp. 692–700, May 1992.

[31] E. Fragniere, A. v. Schaik, and E. A. Vittoz, "Design of an analogue VLSI model of an active cochlea," *Analog Integr. Circuits Signal Process.*, vol. 12, pp. 19–35, 1997.

[32] R. Sarpeshkar, R. F. Lyon, and C. Mead, "A low-power wide-dynamic-range analog VLSI cochlea," *Analog Integr. Circuits Signal Process.*, vol. 16, pp. 245–274, 1998.

[33] V. Chan, S.-C. Liu, and A. v. Schaik, "AEAR EAR: A matched silicon cochlea pair with address event representation interface," *IEEE Trans. Circuits Syst. I, Reg. Papers*, vol. 54, no. 1, pp. 48–59, Jan. 2007.

[34] S.-C. Liu, A. v. Schaik, B. A. Minch, and T. Delbruck, "Asynchronous binaural spatial sensor with 2 x 64 x 4 channel output, 10.1109/TBCAS. 2013.2281834," *IEEE Trans. Biomed. Circuits Syst.*, 2013.

[35] D. S. Freedman, H. I. Cohen, S. Deligeorges, C. Karl, and A. E. Hubbard, "An analog VLSI implementation of the inner hair cell and auditory nerve using a dual AGC model," *IEEE Trans. Biomed. Circuits Syst.*, vol. 8, no. 2, pp. 240–256, Apr. 2014.

[36] W. Germanovix and C. Toumazou, "Design of a micropower current-mode log-domain analog cochlear implant," *IEEE Trans. Circuits Syst. II, Analog Digit. Signal Process.*, vol. 47, no. 10, pp. 1023–1046, Oct. 2000.

[37] J. Georgiou and C. Toumazou, "A 126-μW cochlear chip for a totally implantable system," *IEEE J. Solid-State Circuits*, vol. 40, no. 2, pp. 430–443, Feb. 2005.

[38] R. Sarpeshkar, C. Salthouse, J.-J. Sit, M. W. Baker, S. M. Zhak, T. K.-T. Lu, L. Turicchia, and S. Balster, "An ultra-low-power programmable analog bionic ear processor," *IEEE Trans. Biomed. Eng.*, vol. 52, no. 4, pp. 711–727, Apr. 2005.

[39] A. v. Schaik and E. Fragniere, "Pseudo-voltage domain implementation of a 2-Dimensional silicon cochlea," in *Proc. IEEE Int. Symp. Circuits and Syst.*, 2001, vol. 2, pp. 185–188.

[40] E. Fragniere, "A 100-channel analog CMOS auditory filter bank for speech recognition," in *Proc. IEEE Int. Solid-State Circuits Conf., Dig. Tech. Papers*, 2005, pp. 140–141.

[41] T. J. Hamilton, C. Jin, A. v. Schaik, and J. Tapson, "An active 2-D silicon cochlea," *IEEE Trans. Biomed. Circuits Syst.*, vol. 2, no. 1, pp. 30–43, Mar. 2008.

[42] B. Wen and K. Boahen, "A silicon cochlea with active coupling," *IEEE Trans. Biomed. Circuits Syst.*, vol. 3, no. 6, pp. 444–455, Dec. 2009.

[43] H. Finger and S.-C. Liu, "Estimating the location of a sound source with a spike-timing localization algorithm," in *Proc. IEEE Int. Symp. Circuits and Systems*, 2011, pp. 2461–2464.

[44] C.-H Li, T. Delbruck, and S.-C. Liu, "Real-time speaker identification using the AEREAR2-event-based silicon cochlea," in *Proc. IEEE Int. Symp. Circuits and Systems*, 2012, pp. 1159–1162.

[45] K. H. Wee, L. Turicchia, and R. Sarpeshkar, "An articulatory silicon vocal tract for speech and hearing prostheses," *IEEE Trans. Biomed. Circuits Syst.*, vol. 5, no. 4, pp. 339–346, Aug. 2011.

[46] J.-J. Sit and R. Sarpeshkar, "A cochlear-implant processor for encoding music and lowering stimulation power," *IEEE Pervasive Comput.–Special Issue Implantable Electronics*, vol. 7, no. 1, pp. 40–48, 2008.

[47] W. Ngamkham, C. Sawigun, S. Hiseni, and W. A. Serdijn, "Analog complex gammatone filter for cochlear implant channels," in *Proc. IEEE Int. Symp. Circuits and Systems*, 2010, pp. 969–972.

[48] A. G. Katsiamis, E. M. Drakakis, and R. F. Lyon, "A biomimetic, $4.5\ \mu$W, 120+ dB, log-domain cochlea channel with AGC," *IEEE J. Solid-State Circuits*, vol. 44, no. 3, pp. 1006–1022, Mar. 2009.

[49] M. Banu and Y. Tsividis, "An elliptic continuous-time CMOS filter with on-chip automatic tuning," *IEEE J. Solid-State Circuits*, vol. 20, no. 6, pp. 1114–1121, Dec. 1985.

[50] J. Adut, J. Silva-Martinez, and M. Rocha-Perez, "A 10.7-MHz six-order SC ladder filter in $0.35\ \mu$m CMOS technology," *IEEE Trans. Circuits Syst. I, Reg. Papers*, vol. 53, no. 8, pp. 1625–1635, Aug. 2006.

[51] D. Perry and G. W. Roberts, "The design of log-domain filters based on the operational simulation of LC ladders," *IEEE Trans. Circuits Syst. II, Analog Digit. Signal Process.*, vol. 43, no. 11, pp. 763–774, Nov. 1996.

[52] G. D. Duerden, G. W. Roberts, and M. J. Deen, "A 10 MHz elliptic log-domain filter in a standard CMOS process," in *Proc. IEEE Symp. Circuits and Systems*, 2002, vol. 2, pp. II-5–II-8.

[53] C. Toumazou, J. Ngarmnil, and T. S. Lande, "Micropower log-domain filter for electronic cochlea," *Electron. Lett.*, vol. 30, no. 22, pp. 1839–1841, Oct. 1994.

[54] D. Python and C. C. Enz, "A micropower class-AB CMOS log-domain filter for DECT applications," *IEEE J. Solid-State Circuits*, vol. 36, no. 7, pp. 1067–1075, Jul. 2001.

[55] F. Yang, C. Enz, and G. v. Ruymbeke, "Design of low-power and low-voltage log-domain filters," in *Proc. IEEE Symp. Circuits and Systems*, 1996, vol. 1, pp. 117–120.

[56] C. Psychalinos and S. Vlassis, "On the exact realization of log-domain elliptic filters using the signal flow graph approach," *IEEE Trans. Circuits Syst. II, Analog Digit. Signal Process.*, vol. 49, no. 12, pp. 770–774, Dec. 2002.

[57] E. M. Drakakis, A. J. Payne, C. Toumazou, A. E. J. Ng, and J. I. Sewell, "High-order lowpass and bandpass elliptic log-domain ladder filters," in *Proc. IEEE Symp. Circuits and Systems*, 2001, vol. 1, pp. 141–144.

[58] F. Yuan*, CMOS Active Inductors and Transformers: Principle, Implementation, and Applications*. New York, NY, USA: Springer, 2008.

[59] S. Wang, T. J. Koickal, A. Hamilton, E. Mastropaolo, R. Cheung, and L. Smith, "A floating active inductor based CMOS cochlea filter with high tunability and sharp cut-off," in *Proc. IEEE Symp. Circuits and Systems*, 2013, pp. 193–196.

[60] Y. P. Tsividis*, Operation and Modeling of the MOS transistor*. New York, NY, USA: McGraw-Hill, 1987.

[61] A. B. Williams and F. J. Taylor*, Electronic Filter Design Handbook*. New York, NY, USA: McGraw-Hill, 1995.

[62] C. C. Enz and E. A. Vittoz, *Charge-Based MOS Transistor Modeling: The EKV Model for Low-Power and RFIC Design*. Hoboken, NJ, USA: Wiley, 2006.
[63] E. d. Boer, "Cochlear models and minimum phase," *J. Acoust. Soc. Amer.*, vol. 102, no. 6, pp. 3810–3813, Dec. 1997.
[64] C. A. Shera and J. J. Guinan, "Stimulus-frequency-emission group delay: A test of coherent reflection filtering and a window on cochlear tuning," *J. Acoust. Soc. Amer.*, vol. 113, no. 5, pp. 2762–2772, May 2003.
[65] B. R. Glasberg and B. C. J. Moore, "Derivation of auditory filter shapes from notched-noise data," *Hear. Res.*, vol. 47, no. 1-2, pp. 103–128, Aug. 1990.
[66] S. Ramakrishnan, A. Basu, L. K. Chiu, J. Hasler, D. Anderson, and S. Brink, "Speech processing on a reconfigurable analog platform," *IEEE Trans. Very Large Scale Integr. (VLSI) Syst.*, vol. 22, no. 2, pp. 430–433, Feb. 2014.
[67] R. F. Lyon, A. G. Katsiamis, and E. M. Drakakis, "History and future of auditory filter models," in *Proc. IEEE Int. Symp. Circuits and Systems*, 2010, pp. 3809–3812.
[68] A. G. Katsiamis, E. M. Drakakis, and R. F. Lyon, "Practical gammatone-like filters for auditory processing, doi:10.1155/2007/63685," *EURASIP J. Audio, Speech, Music Process.*, 2007.
[69] B. Gilbert, "The multi-tanh principle: a tutorial overview," *IEEE J. Solid-State Circuits*, vol. 33, no. 1, pp. 2–17, Jan. 1998.

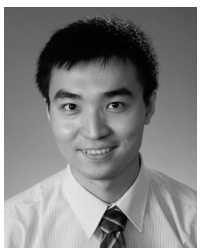

Shiwei Wang (S'13) was born in China in 1987. He received the B.S. degree in electrical engineering from Zhejiang University, Zhejiang, China, in 2010.

Currently, he is working toward the Ph.D degree at the Institute for Integrated Micro and Nano Systems, The University of Edinburgh, Edinburgh, U.K. His research interests include analog VLSI and bio-inspired circuits and systems.

Thomas Jacob Koickal received the Ph.D degree in electronics and electrical communication engineering from the Indian Institute of Technology, Kharagpur, India.

From 1998 to 2002, he was a Scientist at the Control and Guidance Design Group, Indian Space Research Organization, Trivandrum. From 2002 to 2014, he was with the Institute of Micro and Nano Systems, University of Edinburgh, U.K. Currently, he is with Beach Theory, a startup company which he cofounded. His research interests include predictive modeling, time event based computation, neuromorphic systems, and multisensory bio-inspired systems in analog VLSI.

Alister Hamilton is a Senior Lecturer in the discipline of electronics at the School of Engineering, University of Edinburgh, Edinburgh U.K., where he has worked since 1988.

His research interests are in the implementation of neural networks and neuromorphic systems in analog VLSI, and in novel design strategies for programmable analog arrays.

Rebecca Cheung (M'96–SM'02) received first-class honours and the Ph.D degree in electronics and electrical engineering from the University of Glasgow, Glasgow, U.K., in 1986 and 1990, respectively.

In 1986, she was awarded a Croucher Foundation scholarship to study towards a doctoral degree. During her doctoral work, she was a Visiting Researcher at IBM Thomas J. Watson Research Center, Yorktown Heights, NY, USA, where high density plasma etching techniques were developed to form nanostructured GaAs. From 1990 to 2000, she was a Visiting Scientist at the Delft Institute of Microelectronics and Submicron Technology, The Netherlands; the Laboratory for Electromagnetic Fields and Microwave Electronics at ETHZ, Switzerland; and the Nanoelectronics Research Center at the University of Glasgow, working on various topics related to semiconductor technology, process-induced materials damage, mesoscopic physics in SiGe heterostructures, and microwave circuits in InP for gigabit electronics. Additionally, she was a founding member of the Nanostructure Engineering Science and Technology (NEST) Group at the University of Canterbury, New Zealand, in 1998. Currently, she holds a Chair in Nanoelectronics in the School of Engineering at the University of Edinburgh. She has an international reputation for her contribution in the development and application of micro- and nano- fabrication. More recently, her research focuses on bio-inspired micro-electromechanical systems. She has authored over 140 scientific articles with more than 85 peer-reviewed journal papers, including 15 invited review papers, one patent, and one book.

Dr. Cheung serves on numerous scientific panels and committees, has been elected a Fellow of the Royal Society of Edinburgh, and is an Honorary Professor with the School of Engineering and Physical Sciences, Heriot-Watt University, Currie, U.K.

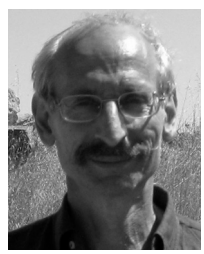

Leslie S. Smith (M'84–SM'04) received the B.Sc. degree in mathematics and the Ph.D. degree in computers from the University of Glasgow, Glagow, U.K., in 1973 and 1982, respectively.

Having worked on parallel systems, he moved on to working on neural networks, gradually exploring both real (biological) and artificial (neuromorphic) implementations. He became interested in the auditory area initially as a source of time-varying data, and remained interested after discovering the problems posed by this area. He was Head of Department at Stirling University, Stirling, U.K, and is currently researching cochlea-like transducers as well as neuroinformatics.